Combining Kohn-Sham and orbital-free density-functional theory for Hugoniot calculations to extreme pressures

Daniel Sheppard, Joel D. Kress, Scott Crockett, Lee A. Collins, and Michael P. Desjarlais

Phys. Rev. E **90**, 063314 — Published 22 December 2014

DOI: 10.1103/PhysRevE.90.063314

Combining Kohn-Sham and orbital-free density-functional theory for Hugoniot calculations to extreme pressures

Daniel Sheppard,[1,*] Joel D. Kress,[1] Scott Crockett,[1]

Lee A. Collins,[1] and Michael P. Desjarlais[2]

[1] *Theoretical Division, Los Alamos National Laboratory, Los Alamos, New Mexico 87545*

[2] *Pulsed Power Sciences, Sandia National Laboratories, Albuquerque, New Mexico 87185*

Abstract

The shock Hugoniot for Lithium 6 Deuteride (^{6}LiD) was calculated *v*ia first principals using Kohn-Sham density functional theory molecular dynamics (KSMD) for temperatures of 0.5-25 eV. The upper limit of 25 eV represents a practical limit where KSMD is no longer computational feasible due to the number of electronic bands which are required to be populated. To push the Hugoniot calculations to higher temperatures we make use of Orbital-Free density functional theory molecular dynamics (OFMD). Thomas-Fermi-Dirac based OFMD gives a poor description of the electronic structure at low temperatures so the initial state is not well defined. We propose a method of bootstrapping the Hugoniot from OFMD to the Hugoniot from KSMD between 10-20 eV where the two methods are in agreement. The combination of KSMD and OFMD allows construction of a first-principles Hugoniot from the initial state to 1000 eV. Theoretical shock-compression results are in good agreement with available experimental data and exhibit the appropriate high temperature limits. We show that unified KSMD/OFMD Hugoniot can be used to assess the quality of the existing equation of state (EOS) models and inform better EOS models based on justifiable physics.

*Electronic address: `danielsheppard@lanl.gov`

I. INTRODUCTION

At present, for an extensive range of temperatures and densities from melt to a fully-ionized plasma, Density Functional Theory Molecular Dynamics [DFT-MD, also known as Q(uantum)MD] provides the most consistent determination of microscopic properties such as equation of state, mass diffusion, viscosity, opacity, and thermal conductivity. Given the nature of the warm dense matter (WDM) regime, the fast-moving electrons require a quantum mechanical treatment through the solution of a Schrödinger-like equation for the complex many-electron wave function from which the basic electronic properties and forces on the ions derive. In turn, the slow-moving ions advance according to classical Newtonian equations-of-motion by standard MD prescriptions. For the electronic component, which computationally dictates the rate-determining step, we employ finite-temperature density functional theory (DFT) formulations in two distinct flavors: the orbital-based Kohn-Sham (KS) and the density-based orbital-free (OF). The computational cost of the KSMD approach confines its applications to temperatures below about 20 eV for matter at ambient solid densities. However, as the density increases so too does the effective temperature range. For example, KSMD has effectively treated hydrogen at 80 g/cm^3 up to a temperature of 800 eV[1, 2]. The KSMD uses highly sophisticated treatments of the electrons that can produce results at the level of quantum chemistry and condensed matter accuracy. For higher temperatures at which quantum effects become less important, we appeal to OFMD with semi-classical approximations to the electron contributions, which in turn smoothly extends into the extreme temperature limit of a hot plasma. The OFMD therefore forms a natural bridge between the low- and high-temperature regimes.

Hugoniots based solely on KSMD simulations have become a common feature since the turn of the millennium [3, 4] with constructions for a variety of materials, for example, N_2 [5], diamond[6], and Xe[7]. However, the above-mentioned limitations have restricted the range of applications. Several recent studies[8–13] have documented a generally smooth transition between the KS and OF regimes for a few species over specific ranges of temperature and densities for selected properties such as equation of state (EOS), mass transport, and conductivities. Wang and Zhang even leverage this overlap to calculate the Hugoniot for H_2 using OFMD[14]. Such auspicious findings call for a systematic examination of the efficacy of generating equation-of-state (EOS) tables or Hugoniots using both formulations

in tandem to cover a broad expanse of phase space. In addition, the role such *ab initio* approaches might play in providing better data for the generation of empirical EOSs needs further clarification. To examine some of these possibilities, we focus on the ^{6}LiD system, which presents sufficient complexities to provide a illustrative example.

The remainder of the paper includes three sections. In Section II, we briefly describe the KSMD and OFMD approaches as well as the matching procedure for systematically joining the two. We will summarize available LiD shock data and also discuss the construction of empirical equations of state. The next section presents the results of a set of calculations for the principal Hugoniot of ^{6}LiD that demonstrate the efficacy of bootstrapping the OFMD from the KSMD and gives a comparison with the empirical models. Section IV summarizes our findings and observations.

II. FORMULATION

A. Quantum Molecular Dynamics

For both flavors of the QMD, we consider a cubic cell of volume (V=L^3) of N_i ions and N_e electrons, periodically-replicated throughout space to represent a fluid and invoke the Born-Oppenheimer approximation to separate the electronic and nuclear motions. The nuclei move according to classical equations of motion (EOM) in response to a force on an ion from the interactions with other ions and a quantal contribution from the electrons at a fixed ion configuration [$\mathbf{R}_i$, i=1,N_i]. The repetition of this two-step process over a series of timesteps constitutes the molecular dynamics prescription that produces a trajectory of ionic positions and velocities as well as an electronic wavefunction $\Psi(\mathbf{r}_j, \mathbf{R}_i, t)$ and density $n_e = \int \Psi^* \Psi d\mathbf{r}$ with the electrons occupying positions $\mathbf{r} \equiv [\mathbf{r}_1, ..., \mathbf{r}_{N_e}]$. Various static, dynamic, and conductive properties derive from the direct trajectory information. Local thermodynamic equilibrium results in equal electron and ion temperatures ($T_e = T_i = T$) with the former held fixed, and the latter maintained through an isokinetic thermostat[15].

The KS-DFT calculations employed the Vienna Ab initio Simulation Package, VASP [16–18] with the electronic wavefunctions described by a plane-wave basis set within the Generalized Gradient Approximation (GGA) for the Perdew-Burke-Ernzerhof[19] (PBE) exchange-correlation having the ion-electron interaction represented by projector augmented

wave (PAW) potentials [20] in the all-electron GW forms. The energy cut-offs for plane waves and augmentation charges were set to 823 eV and 1706 eV, respectively. These values correspond to the optimum cut-off when building the PAW, with kinetic energy errors of 0.0078 eV/atom for Li and 0.0026 eV/atom for D. The standard MD simulation employed the Baldereschi mean-value point[21] with 32 ^{6}Li and 32 D atoms. The timesteps varied from 0.025 fs to 0.2 fs, depending on the temperature, with trajectory lengths of thousands of time steps. We also performed calculations with larger numbers of atoms as well as higher energy cut-offs and observed only small differences of a few per cent.

In OFMD simulations[8, 9, 22, 23], the force due to the electrons arises from the minimizations of a finite-temperature orbital-free density functional(OF-DFT) in terms of the electron density $n_e(\mathbf{r})$ of the form:

$$F_e[n_e] = T_0[n_e] + U_{en}[n_e] + U_{ee}[n_e] + F_{xc}[n_e]. \tag{1}$$

We operate in a Thomas-Fermi-Dirac mode with the kinetic-entropic $T_0[n_e]$ of Perrot [24], the electron-ion interaction U_{en} from a regularization prescription[8], the electron-electron Hartree contribution U_{ee}, and the exchange-correlation term F_{xc} from a local density Perdew-Zunger form[25]. The number of plane waves describing the local electronic density is then adjusted to converge the thermodynamic properties to within 1%. The OF procedure treats all electrons on an equal footing, albeit approximately, with no distinction between bound and ionized electrons.

The molecular dynamics simulations employed 64 ^{6}Li and 64 D atoms with timesteps varying for 0.01 fs to 0.1 fs according to the temperature with trajectories extending over 10^4 timesteps. For a given temperature and density, the mean time between collisions is estimated from the average interatomic distance (determined from the atomic volume) and the thermal speeds of Li and D. The timestep is chosen to accurately integrate the equations of motion of the ions between collisions and accurately resolve the fluctuations in the pressure. The total pressure was converged to less than 0.5% for timestep and to 3% or less for system size. Ref. 13 extensively details OFMD simulations of LiH for T up to 10 keV and was used to inform parameters for OFMD calculations in this work. Details for the analysis of radial distribution functions are included in the Appendix. All structures in this temperature and density range resemble that of a simple liquid[10].

B. Hugoniot match and bootstrapping methodology

The Rankine-Hugoniot jump conditions describe the states on either side of the shock wave as

$$U - U_0 = \frac{1}{2}(P + P_0)(\bar{V} - \bar{V}_0), \tag{2}$$

where U is the internal energy, P is the pressure, and the specific volume is the reciprocal of the density $\bar{V} = 1/\rho$. To construct the Hugoniot for KSMD, we first calculate the initial state (U_0, ρ_0, and P_0). For ^{6}LiD, ρ_0=0.80 g/cm^3 is chosen to match the experimental density from Marsh[26], P_0=0 is assumed, and U_0 is then calculated from the T=0 solid. The ambient Hugoniot reference state included corrections for the zero-point energy effects, determined from the phonon density of states [27] and quasi-harmonic theory. The final conditions $\{U$, ρ, and $P\}$ representing solutions to Eq. (2) delineate the shock Hugoniot. The internal energy $U = \frac{3}{2}k_BT + \frac{E}{N}$ is the sum of ion kinetic energy and the time-averaged DFT internal energy E, where k_B is the Boltzmann constant and N is the number of atoms in the supercell. Similarly, $P = P_e + Nk_BT$, is the sum of the ion kinetic contribution and the electronic pressure, P_e derived from Hellmann-Feynman forces. In lieu of directly simulating the shock Hugoniot points, the steady-state properties P and U were fit to a quadratic as a function of T for a grid of isochoric simulations; these fits in turn were used to solve Eq. (2). High compression necessitates an interpolate as a function of density.

To push the shock Hugoniot to extreme pressures, we use OFMD to calculate our steady-state properties. For materials and molecular liquids at low temperatures and ambient densities typically representative of the initial state in a Hugoniot experiment, the Thomas-Fermi and Thomas-Fermi-Dirac density functional theories predict zero and negligible cohesive energy, respectively, in poor agreement with experimental observations. Although adequate for plasmas, this severe underestimation of binding forces in molecules and solids is due to an inadequacy of the effective electronic response properties of these functionals under these conditions[28]. Therefore, we have no way of directly simulating U_0 within the Thomas-Fermi-Dirac framework using OF-DFT. To circumvent this issue, we choose to bootstrap our OF shock Hugoniot from the KS shock Hugoniot where the quality of the two methods have the highest overlap. In this overlap region, for a given $\bar{V}$ point on the KS-Hugoniot, the temperature of the OFMD calculation is adjusted to obtain a good pressure match between the OF and KS calculations. We then assume that this OFMD point is on the shock

Hugoniot and using Eq. (2) are able to extract the U_0 for the OFMD calculations. With the initial state for OFMD known, the rest of the shock Hugoniot is calculated using the same procedure as for the lower pressure KS points. Wang and Zhang were able to simulate the Hugoniot for hydrogen using U_0 from KS calculations because of a fortuitous match of both U and P at high temperatures[14]. Our bootstrapping technique does not require a common energy reference for KS and OF implementations thus making the method general.

C. Experimental measurements of ^{6}LiD

The main body of experimental Hugoniot data available was compiled by Marsh[26]. In these experiments, high explosive was used to drive the shock; the shock velocity was measured by a sweeping-image camera and a shock-impedance matching technique[29] was used to extract particle speed using a 2024 Al standard. Shock velocities were measured for pressed samples of ^{6}LiD (ρ_0=0.45 0.80 g/cm^3) for pressures up to 50 GPa. The same experiments were preformed on isotopic variants including: ^{7}LiD, ^{7}LiH, ^{6}LiH, ^{n}LiH and ^{n}LiD, where n indicates natural isotopic abundance (n=6.94amu). These experiments provided a range of porous Hugoniot results, which helped constrain the EOS at low pressures. In addition, there are also nuclear-explosive-driven shocks where impedance matching (NIM) to a Mo standard was used to obtain the Hugoniot for ^{n}LiD[30] and ^{n}LiH[31]. In these experiments ^{n}LiD was shocked to a pressure of 946 and 1038 GPa and ^{n}LiH to a pressure of 1225 GPa.

D. Empirical EOS

One of our immediate purposes entails utilizing *ab initio* techniques (QMD) to calibrate a wide range of EOS. The theoretical calculations serve as an analog to experimental data over ranges not typically reached by experiment. However, just as with experiment, these *ab initio* calculations do not directly correspond to parameters in our models used to calculate EOS. Therefore, we need to understand the relationship of the models and thermodynamics in order to utilize the results. The EOS modeling for LiD is based on a standard three-term decomposition of a Helmholtz free energy,

$$A(\rho, T) = A_{cc}(\rho) + A_{ion}(\rho, T) + A_{ele}(\rho, T). \tag{3}$$

The three-term decomposition consists of a zero temperature cold curve, A_{cc}, as well as ion thermal, A_{ion} and electron thermal, A_{ele}, components. The cold curve is representative of the nuclei in fixed equilibrium positions with electrons in their ground state. The ion thermal part encompasses both the zero-point and the thermal motion of the nuclei and is given by a Debye model at low temperature with a correction for the fluid component at temperatures above melt. The electron thermal part accounts for the thermal excitation of the electrons out of their ground state and is calculated using a Thomas-Fermi-Dirac average-atom model for each element with the individual thermal components appropriately combined through an additive volume mixture procedure to yield a result for the compound LiD.

Typical equation of state models require a variety of experimental data and theoretically-derived calculations in order to constrain the various model parameters. The cold curve model consists of a Rose-Vinet analytic expression, fit to match experiment at low pressure (diamond anvil cell and Hugoniot), which extends into the Thomas-Fermi-Dirac average-atom model at high pressure. The Debye model parameters are chosen to match the thermal expansion, specific heat, and high pressure Hugoniot data. All too often the data and calculations remain limited in range or accuracy, thereby only weakly constraining the models. Older Hugoniot data at extremely high pressure for LiD has large error bars and larger scatter. This leaves the parameters controlling the high compression response of our models unconstrained. The latest Z-pinch and laser-driven experiments provide only compression but not thermal information.

To illustrate the effects of weak experimental constraints on the high temperature EOS, we examine two older SESAME[32] models for ^{6}LiD: SESAME, 7245 (1985) and SESAME 7247 (2006). SESAME 7245 was constructed using only the principal Hugoniot data while 7247 was parameterized based on principal and porous Hugoniot data (Sec. II C). SESAME 7247 utilizes a cold curve based on a Mie-Gruneisen approximation with a quadratic fit to the shock and particle velocity, and the ion thermal contribution is based on a Debye model with a correction for the liquid specific heat beyond the melt temperature with the Debye temperature set to 1050K. The Thomas-Fermi-Dirac average-atom model is used to calculate the thermal electronic component of each element and later combined using an additive volume mixing procedure. SESAME 7245 was constructed in a similar way: the EOS was fit via a Mie-Gruneisen approximation, a Debye model was used for the ion thermal contribution, and the electron thermal contribution was generated from an average atom INFERNO

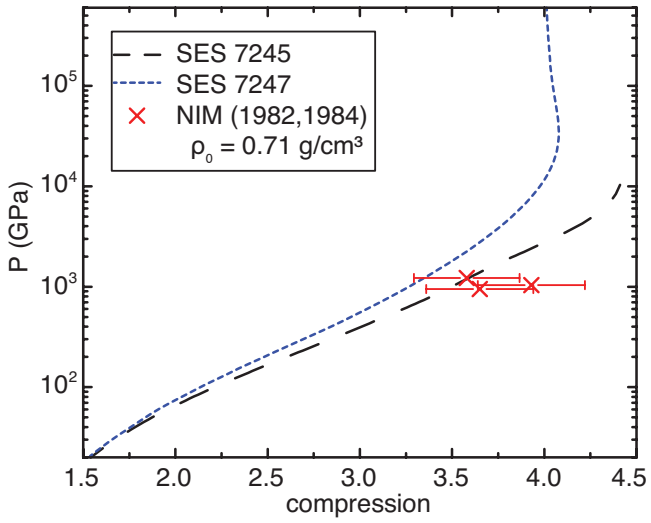

FIG. 1: (Color online) Porous Hugoniot, ρ_0=0.71g/cm^3, of ^{6}LiD in compression space ($\eta = \rho/\rho_0$). SESAME 7245 shown in dashed black and SESAME 7247 shown in dotted blue. Isotopicly scaled NIM[30, 31] data shown as red crosses.

model[33, 34].

Fig. 1 shows NIM results compared to SESAME[32] EOS models 7245 an 7247. The initial and final densities for the NIM data was isotopically scaled to their corresponding ^{6}LiD densities so a direct comparison with ^{6}LiD SESAME EOS can be made. The isotopically scaled ρ_0 for both NIM shots is 0.71 g/cm^3. The porous Hugoniot for SESAME 7245 and 7247 exhibit identical behavior at low compression and pressures. The thermal electronic part of SESAME 7245 is incomplete and fails to converge to the proper ideal gas limit of ions plus electrons. SESAME 7247 converges to the appropriate limit but is noticeably stiffer than 7245. Given the error bars in the NIM data, it could be subjectively argued that SESAME 7245 is also too stiff. We will show that using KSMD and OFMD, the high temperature EOS can be systematically constrained based on justifiable physics rather than fit within huge error bars. A new ^{6}LiD EOS SESAME 7360 will be presented based on *ab initio* results in conjunction with lower pressure experimental results.

III. RESULTS AND DISCUSSION

We show in Fig. 2 an illustration of the bootstrap technique, described in Sec. II B, for constructing the composite ^{6}LiD Hugoniot in compression space ($\eta = \rho/\rho_0$) for a solid

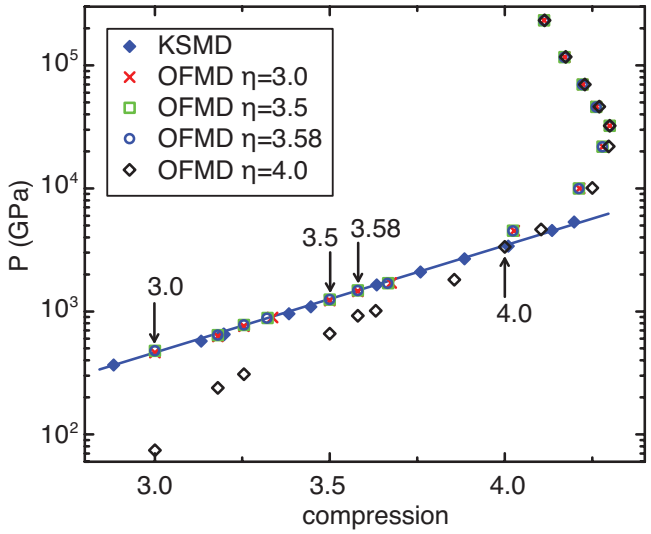

FIG. 2: (Color online) Bootstrap illustration for the ^{6}LiD Hugoniot with initial density $\rho_0 = 0.80$ g/cm^3. KSMD results appear as solid blue diamonds. The line is drawn to guide the eye along the KSMD points. The OFMD results represent the sensitivity to the compression at which the matching procedure was applied, ranging from 3.0 to 4.0.

density ^{6}LiD ($\rho_0 = 0.80$ g/cm^3). KSMD calculations, shown as solid blue diamonds, range over compressions from 3.0 to 4.5, which correspond to temperatures between 0.6 eV to 28 eV. The continuation of the Hugoniot with OFMD is shown for matching compressions of $\eta = 3.0$ (red crosses), 3.5 (green squares), 3.58 (open blue circles), and 4.0 (open black diamonds). For the lowest three matching compressions, the OFMD predictions are robust to choice of bootstrapped location, yielding a difference of OFMD U_0 of $\sim$0.1 eV (0.07%), and less than 3.5% ($\delta P < 60 GPa$) in the pressure with the largest differences at the lowest compressions. At $\eta > 3.6$, the Hugoniot from KSMD starts to soften due to the onset of ionization of the Li 1s electrons. In the vicinity of the 1s ionization the OF-DFT, based on Thomas-Fermi-Dirac, and KS-DFT, which has a true shell structure, are likely not well matched making the region less that ideal for bootstrapping location. At a chosen bootstrap compression of η=4.0, the high pressure results still agree well with those matched from lower compressions; the comparison at low compressions suffers because P must balance a 2.6 eV difference in U_0 from Eq. (2). This same Hugoniot softening is seen when using Purgatorio[34], a relativistic average atom code, for the electronic part of an EOS model compared to using Thomas-Fermi-Dirac. To avoid influencing the predicted Hugoniot with

this Li 1s ionization difference, and to maximize the OFMD/KSMD overlap region, we will use the average value of U_0 found from bootstrapping to the KSMD at three points (η=3.0, 3.5, and 3.58) on the full density Hugoniot used to solve Eq. (2).

We used this fully *ab initio* Hugoniot, built from KS and OF, to constrain a new EOS for ^{6}LiD. SESAME 7360 utilizes a cold curve based on a Mie-Gruneisen approximation with a quadratic fit to the shock, u_s, and particle velocity, u_p, Hugoniot data ($u_s = 6.3913 + 1.2041u_p - 0.011906{u_p}^2$). The Gruneisen parameter (γ) was set to 1.108 based on porous Hugoniot data[26] and was confirmed to match thermal expansion data[35]. The density derivative ($\gamma' = \frac{d\gamma}{d\rho}$) is set to a value of -1.45 to match porous OFMD results. The ion thermal contribution is based on a Debye model with a correction for the liquid specific heat beyond the melt temperature with the Debye temperature set to 1050K. The Thomas-Fermi-Dirac model is used to calculate the thermal electronic component, Li and D, and later combined using an additive volume mix procedure. OFMD results provide electron thermal and ion thermal contributions beyond the quasi-harmonic approximation. SESAME 7360 and SESAME 7247 use the exact same models but γ and γ' have the correct behavior in the formulation for SESAME 7360. Using smooth equations to fit the EOS as prescribed in Sec. II D insures that no derivative discontinuities are introduced from the bootstrapping procedure.

In Fig. 3, we compare the Hugoniots generated from the KSMD, the bootstrapped OFMD, SESAME models 7245 and 7360, and the LASL shock data[26]. By design, SESAME 7360 agrees with the composite OFMD calculations across the full range of compressions. Staring at 300 GPa SESAME 7360 departs from the KS results for $\eta > 4$ where the ionization of the Li 1s orbitals becomes important. The SESAME 7360 EOS has just reached the ideal gas limit of ions plus electrons [36] on the Hugoniot ($\eta = 4$ as $T \to \infty$) in the upper right hand corner of Fig. 3 (around $P = 6 \times 10^5$ GPa). As the pressure decreases from here, the non-ideal contribution to the EOS slowly contributes consistent with the high temperature behavior observed in the cusp-like constraints approximation [37] and path integral Monte Carlo simulations [38] for the deuterium (D_2) Hugoniot.

In Fig. 4 we compare temperatures at various Hugoniot points for several models. Note that temperature agreement was not guaranteed by the bootstrapping procedure described in Sec. II B. One might expect large differences in temperature between OFMD and KS results because temperature was the free parameter used to ensure pressure matched at a given

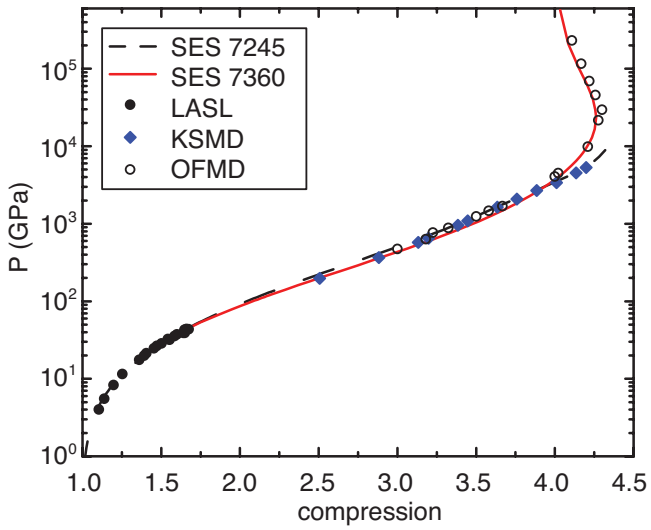

FIG. 3: (Color online) Hugoniot for ^{6}LiD with initial density $\rho_0 = 0.80$ g/cm^3 as a function of compression ($\eta = \rho/\rho_0$). Black filled circles represent LASL data[26], blue diamonds the KSMD calculations, and open circles the OFMD results fit to KSMD results at the average U_0 for $\eta = 3.0$, 3.5, and 3.58. Dashed black and solid red solid lines are SESAME EOS 7245 and 7360, respectively.

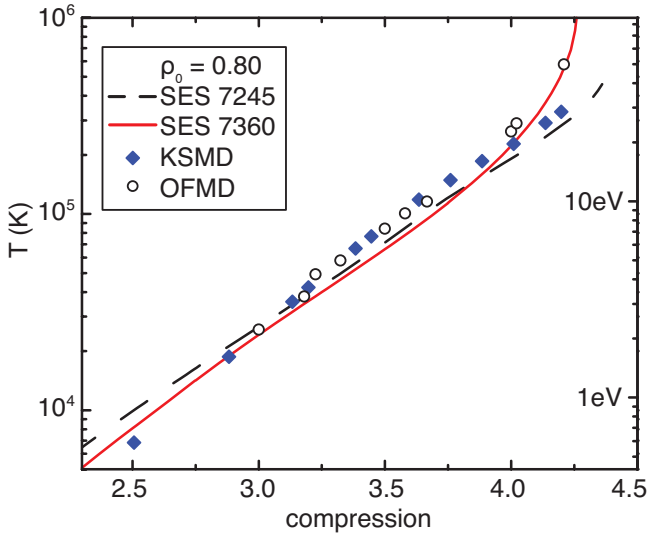

FIG. 4: (Color online) Hugoniot, as a function of compression ($\eta = \rho/\rho_0$) for ^{6}LiD with initial density $\rho_0 = 0.80$ g/cm^3. Blue diamonds the KSMD calculations, and open circles the OFMD results bootstrapped to KSMD results. Dashed black and solid red lines are SESAME EOS 7245 and 7360, respectively.

density. The fact that temperatures match for KS and OF in the overlap region indicates that both methods are adequate to describe the physics in this phase space. This overlap region allows the smooth transition from one DFT into the next. The same arguments can be made for temperature agreement between the OFMD and SESAME 7360 to higher pressures. Temperature serves as a good intrinsic check for the EOS among the models since in some cases Hugoniot values can coincide but for different temperatures.

To calculate the OFMD Hugoniot of porous ^{6}LiD samples requires a knowledge of U_0. For the purposes of this paper, U_0 for a porous sample is assumed to equal to U_0 of the full density sample. This approximation translates to the physical assumption that the porous sample has the same bond lengths as the full density sample with bubbles separating sections of full density ^{6}LiD. Furthermore, it assumes no contribution from the surfaces of the bubbles. Using this approximation, the same average value of U_0 from bootstrapping at three compressions is also used for porous samples. The Hugoniots from SESAME 7360 are calculated under the same approximation of constant U_0. Initial densities for porous calculations were chosen to match those for LASL experiments[26] ($\rho_0 = 0.45, 0.58, 0.66,$ and 0.80 g/cm^3). These experimental points are shown in the lower left hand corner of Fig. 5 as solid points. These experiments are in good agreement with the porous SESAME Hugoniot calculations lending credibility to a constant U_0 approximation. Comparison to porous shock data is an important check for any EOS because the thermal electronic and thermal ionic parts of Eq. 3 dominate where as in the principal Hugoniot the cold curve strongly influences the pressure/density behavior.

Figure 5 also shows NIM experimental results[30, 31] described in Sec. II C. NIM results are shown as crosses in Fig. 5. Given the large error bars in compression for the NIM experiments and the agreement between KS and OF DFT we feel confident that OFMD results should be predominately used to inform the ^{6}LiD EOS at extreme pressures.

IV. SUMMARY

The shock Hugoniot for Lithium 6 Deuteride was calculated *v*ia first principals to a temperature of 1000 eV. This was achieved using a combination of KSMD and OFMD. A new robust method was developed for bootstrapping the high temperature OFMD Hugoniot to the Hugoniot calculated from KSMD. This bootstrapping procedure facilitates a smooth

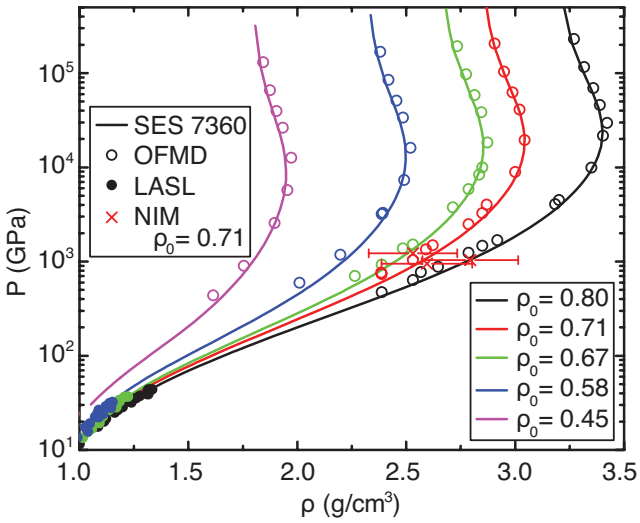

FIG. 5: (Color online) Hugoniot for porous ^{6}LiD. Solid lines are SESAME 7260, open circles are OFMD results, solid circles are LASL data[26], and crosses are nuclear impedance matching experiments[30, 31]. From left to right porous Hugoniot calculations in ascending order with $\rho_0 = 0.45, 0.58, 0.66, 0.71,$ and 0.80 g/cm^3.

transition along the Hugoniot between an orbital based quantum treatment of electrons and Thomas-Femri-Dirac electronic treatment. This first principles Hugoniot is then used to constrain a new EOS for ^{6}LiD, SESAME 7360. This new EOS agrees better with high pressure experimental measurements than its recent predecessor, SESAME 7247, while extending the range of the table well above the legacy EOS, SESAME 7245.

Appendix

The efficacy of the our choice of time steps for the molecular dynamics simulations is demonstrated by examining the radial distribution functions (RDF) at a density of 3.152 g/cm^3 and at our highest temperature of 100eV in Fig. 6. The usual convention for the choice of an effective time step dictates a sufficient number of steps (10-20) to cover a mean separation determined by the density for a mean velocity set by the temperature. Such a choice assures the trajectory avoids aberrant close approach and unphysical forces. Fig. 6a shows the RDFs over the usual range [0, $\frac{L}{2}$]with a typical bin size of 0.05 bohr, where L is the length of the periodic box. The functions rise smoothly from zero at the origin to an asymptotic value of unity, exhibiting no signatures of structure (peaks), resembling the

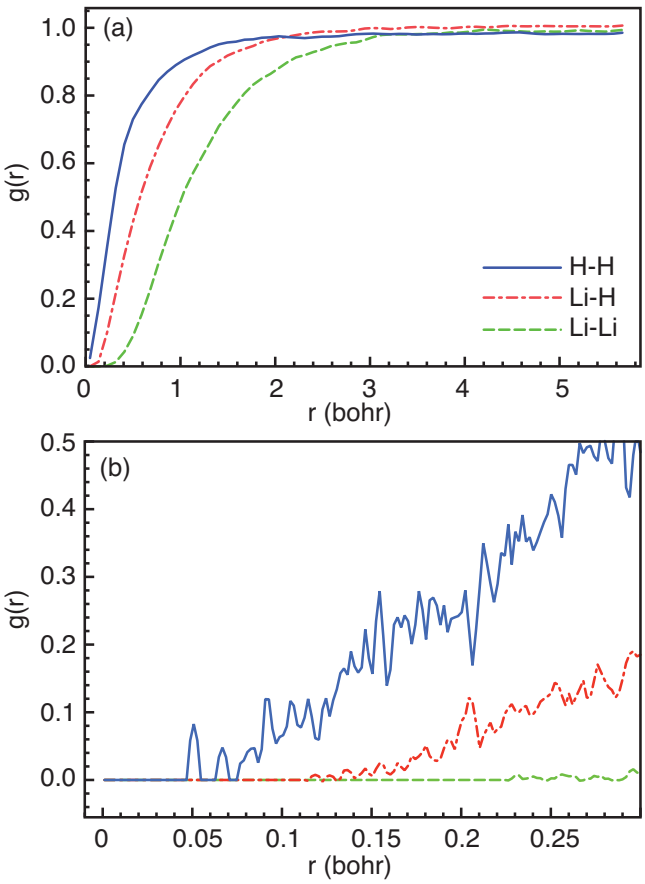

FIG. 6: (Color online) The radial distribution functions [g(r)] for LiH at a temperature of 100eV and a density of 3.152 g/cm^3. The Li-Li (green, dash), Li-H (red, dash-dot), and H-H (blue, solid) functions displayed over the full range (a) with bins of 0.05 bohr and for short-range (b) with bins of 0.001 bohr.

behavior of a simple liquid. In Fig. 6b, we investigate the region very near the origin to ascertain the minimum approach of the various species. In order to reveal the behavior in this regime, bins of very small extent (0.001 bohr) are required, which in turn produces a noisy RDF. The results indicate, even for the lightest species H, that the atoms remain at reasonable separations throughout the simulation and that the time step is adequate to faithfully follow the collisional dynamics. The results at 12eV and 20eV show similar behavior.

Acknowledgments

This work was performed under the auspices of Los Alamos National Laboratory, which is operated by Los Alamos National Security, LLC, for the National Nuclear Security Administration of the U.S. Department of Energy under Contract No. DE-AC52-06NA25396.

---

[1] V. Recoules, F. Lambert, A. Decoster, B. Canaud, and J. Clérouin, Phys. Rev. Lett. **102**, 075002 (2009).

[2] F. Lambert, V. Recoules, A. Decoster, J. Clérouin, and M. Desjarlais, Phys. Plasmas **18**, 056303 (2011).

[3] T. J. Lenosky, S. R. Bickham, J. D. Kress, and L. A. Collins, Phys. Rev. B **61**, 1 (2000).

[4] M. P. Desjarlais, Phys. Rev. B **68**, 064204 (2003).

[5] J. D. Kress, S. Mazevet, L. A. Collins, and W. W. Wood, Phys. Rev. B **63**, 024203 (2000).

[6] N. A. Romero and W. D. Mattson, Phys. Rev. B **76**, 214113 (2007).

[7] S. Root, R. J. Magyar, J. H. Carpenter, D. L. Hanson, and T. R. Mattsson, Phys. Rev. Lett. **105**, 085501 (2010).

[8] F. Lambert, J. Clérouin, and G. Zérah, Phys. Rev. E **73**, 016403 (2006).

[9] S. Mazevet, F. Lambert, F. Bottin, G. Zérah, and J. Clérouin, Phys. Rev. E **75**, 056404 (2007).

[10] D. A. Horner, F. Lambert, J. D. Kress, and L. A. Collins, Phys. Rev. B **80**, 024305 (2009).

[11] F. Lambert and V. Recoules, Phys. Rev. E **86**, 026405 (2012).

[12] J.-F. Daniel, L. Kazandijan, and G. Zérah, Phys. Plasmas **19**, 122712 (2012).

[13] L. Burakovsky, C. Ticknor, J. D. Kress, L. A. Collins, and F. Lambert, Phys. Rev. E **87**, 023104 (2013).

[14] C. Wang and P. Zhang, Phys. Plasmas **20**, 092703 (2013).

[15] P. Murray, G. Martyna, and M. Tuckerman, J. Chem. Phys. **118**, 2510 (2003).

[16] G. Kresse and J. Hafner, Phys. Rev. B **47**, R558 (1993).

[17] G. Kresse and J. Furthmüller, Comput. Mater. Sci. **6**, 15 (1996).

[18] G. Kresse and J. Furthmüller, Phys. Rev. B **54**, 11169 (1996).

[19] J. P. Perdew, K. Burke, and M. Ernzerhof, Phys. Rev. Lett. **77**, 3865 (1996).

[20] G. Kresse and D. Joubert, Phys. Rev. B **59**, 1758 (1999).

[21] A. Baldereschi, Phys. Rev. B **7**, 5212 (1973).

[22] J. Clérouin, E. L. Pollock, and G. Zérah, Phys. Rev. A **46**, 5130 (1992).

[23] F. Lambert, J. Clérouin, J.-F. Danel, L. Kazandjian, and G. Zérah, Phys. Rev. E **77**, 026402 (2008).

[24] F. Perrot, Phys. Rev. A **20**, 586 (1979).

[25] J. P. Perdew and A. Zunger, Phys. Rev. B **23**, 5048 (1981).

[26] S. P. Marsh, *LASL Shock Huginiot Data* (University of California Press, Berkeley CA, 1980).

[27] D. Alfe, Comp. Phys. Comm. **180**, 2622 (2009).

[28] M. Pearson, E. Smargiassi, and P. A. Madden, J. Phys.: Condens. Matter **5**, 3221 (1993).

[29] J. M. Walsh and T. H. Christian, Phys. Rev. **97**, 1544 (1954).

[30] C. E. Ragan III, Phys. Rev. A **25**, 3360 (1982).

[31] C. E. Ragan III, Phys. Rev. A **29**, 1391 (1984).

[32] S. P. Lyon and J. D. Johnson, Tech. Rep. LA-UR-92-3407, SESAME: The Los Alamos National Laboratory Equation of State Database (1992).

[33] D. A. Liberman, Phys. Rev. B **20**, 4981 (1979).

[34] B. Wilson, V. Sonnad, P. Sterne, and W. Isaacs, J. Quant. Spectrosc. Radiat. Transfer **99**, 658 (2006).

[35] J. Zhang, Y. Zhao, Y. Wang, and L. Daemen, J. Appl. Phys. **103**, 093513 (2008).

[36] E. L. Pollock, J. Computer-Aided Mats. Design **5**, 163 (1998).

[37] K. Nagao, S. A. Bonev, and N. W. Ashcroft, Phys. Rev. B **64**, 224111 (2001).

[38] B. Militzer and D. M. Ceperley, Phys. Rev. Lett. **85**, 1890 (2000).